Chem. Pharm. Bull. **73**, 213–226 (2025) Vol. 73, No. 3
https://doi.org/10.1248/cpb.c24-00710

Regular Article

Evaluation of Time-Dependent Deformation Behavior of Pharmaceutical Excipients in the Tableting Process

Daisuke Mizunaga*[,a] and Satoru Watano[b]

[a]*CMC Headquarters, Department of Formulation Research and Development, Otsuka Pharmaceutical Co., Ltd., 13 Minami, Shishitoki, Matsudani, Itano-cho, Itano-gun, Tokushima 779–0195, Japan: and* [b]*College of Engineering, Graduate School of Engineering, Osaka Metropolitan University, 1–1 Gakuen-cho, Naka-ku, Sakai 599–8531, Japan.*
*Correspondence: Mizunaga.Daisuke@otsuka.jp

Received October 22, 2024; accepted January 8, 2025

Tableting is a critical process in the manufacture of pharmaceutical tablets that directly influences product quality. Ensuring consistent quality between the research and development phase and commercial-scale production is essential during scale-up. In this study, we investigated methods for evaluating time-dependent deformation behavior using four excipients that exhibit different compression deformation behaviors. Dicalcium phosphate dihydrate (DCPD) shows no viscoelasticity, whereas lactose monohydrate (LAC), cornstarch (CS), and microcrystalline cellulose (MCC) exhibit viscoelasticity and viscoplasticity, although the degree of viscosity varies between them. In addition to investigating the known strain rate sensitivity (SRS), we performed mechanical energy evaluation based on the area under the force–displacement curve and stress relaxation tests. A trapezoid waveform was applied during the test, with loading punch speeds of 0.5 and 100 mm/s, and a dwell time of 4.5 s. The SRS value for DCPD approached approximately one, indicating no speed dependence, and the SRS increased in the order of LAC < MCC < CS, consistent with previous studies that used a saw-tooth waveform. Among the mechanical energies, the ratio of plastic flow energy to plastic energy, which depends on dwell time, followed a similar trend to SRS for the three materials other than DCPD. We conclude that axial stress relaxation is affected by machine deformation, whereas radial stress relaxation provides insight into the viscous behavior of the material. Under the test conditions, the effects of the punch-displacement profile and compression pressure on the mechanical energy and stress relaxation were more pronounced than those of SRS.

Key words punch speed, strain rate sensitivity, stress relaxation, plastic flow energy, viscosity

Introduction

Tableting is a widely used process in the pharmaceutical industry and plays a crucial role in determining the quality of the final product. Typically, tableting is performed using a rotary tablet press, where dies attached to a rotating turret interact with the upper and lower punches that move along a cam track. As the turret rotates, the steps execute the die filling, loading, unloading, and ejection stages within a single rotation cycle. The time required for the loading and unloading phases depends on the turret rotation speed because these stages occur while the punches traverse beneath the pressure rolls. A critical consideration during scale-up is the fact that the compression time in a commercial-scale rotary tablet press is significantly shorter than that in a research and development (R&D)-scale press owing to the machine's geometric design.[1)]

To understand the performance of raw materials during tableting, it is crucial to assess their behavior during the tableting process. During uniaxial compression of pharmaceutical powders, various deformation behaviors are exhibited by the powder. These behaviors depend on the material properties of the powder and the compression conditions and are mainly classified into plastic and elastic deformation. Plastic deformation refers to irreversible changes in shape in which the material is altered by an external force and does not return to its original state once the force is removed. This phenomenon occurs when a material exceeds its yield stress. During compression, the powder undergoes plastic deformation, resulting in an increase in density and a decrease in volume. In contrast, elastic deformation is a reversible deformation that allows the material to return to its original shape once the external force is removed. This type of deformation occurs when the stress is below the yield stress of the material and reflects the temporary response of the internal structure of the material to stress. As the compression of pharmaceutical powders progresses, the properties of the compacted mass become more dominant than those of the individual particles owing to the increase in density. Furthermore, time-dependent deformation behavior, such as viscous deformation, becomes increasingly significant as compression continues. This refers to deformation that gradually develops as a result of a sustained external force. Viscoplastic deformation refers to a phenomenon in which the material flows and deforms over time, failing to return to its original state even after unloading. This viscous behavior is particularly noticeable in long-duration compression and retention tests.[2)] The concepts of viscoplasticity and viscoelasticity are crucial when examining the time-dependent deformation

characteristics. Viscoplasticity refers to irreversible deformation that occurs over time due to the effects of viscosity, in addition to plastic deformation. This phenomenon was evidenced by the gradual increase in the density of pharmaceutical powders during the compression process. On the other hand, viscoelasticity is a behavior that combines elastic deformation with viscosity, exhibiting the property of partially delayed deformation when an external force is applied and gradually returning to its original state over time. The interactions between plasticity, elasticity, and time-dependent deformation, such as viscosity, govern the compression process of pharmaceutical powders. Understanding these deformation behaviors is essential for determining the optimal tableting conditions and is a critical factor that directly influences the physical properties and performance of tablets. Plastic flow phenomena arise from the viscoplasticity exhibited during uniaxial compression and are detected as changes in punch displacement that occur after the maximum force is reached on the force–displacement plot. The assessment of plastic flow phenomena is often accomplished through mathematical analysis of stress relaxation curves to estimate the elastic and viscous components separately or by comparing the stress relaxation curves of different raw materials.[3–6] Although stress relaxation tests are relatively easy to perform, the conditions under which they are conducted significantly influence the results. For example, stress relaxation has been observed during the slow-filling phase, and the time allotted for relaxation analysis has a considerable impact on the evaluation of stress relaxation curves.[4,7]

Several studies have employed the mechanical energy associated with compression as a metric to quantitatively evaluate the effect of tableting speed on material deformation properties. Typically, mechanical energy is estimated from the area under the force–displacement curve derived from a uniaxial compression test,[8] and the ratio of elastic to plastic energy is correlated with elastic recovery. This is the primary cause of tablet failure.[9–12] There is a segment in the force–displacement curve where compression continues slightly despite a decrease in force after the peak. The area under the curve (*AUC*) in this segment is termed the plastic flow energy.[9,13–15] A few studies have focused on plastic flow energy; however, it has been recognized as a component of plastic energy. This classification is appropriate, considering that plasticity involves time-dependent plastic deformation. In studies using instrumented rotary tablet presses, research has been reported that focuses on the area corresponding to the compression stagnation period of the force–time curve. Antikainen and Yliruusi used an eccentric tablet press, and from the force–displacement curves, they defined the ratio of plastic flow energy to the sum of plastic energy and plastic flow energy as the plasticity factor, while elastic energy was defined as the elasticity factor.[9] This methodology effectively revealed the deformation properties, including plastic flow, brittle fracture, and elastic recovery of lactose monohydrate (LAC), microcrystalline cellulose (MCC), cornstarch (CS), and dicalcium phosphate dehydrate (DCPD). Although plastic flow energy has been recognized in previous studies, it has seldom been the focus of research. Oates and Michel suggested that the peak offset time, derived from the area under the force-time curve, serves as a metric for plastic flow,[16] a concept supported by findings from subsequent studies.[17,18]

One commonly used metric for evaluating punch speed-dependent deformation behavior is the strain rate sensitivity (SRS) index.[19] The SRS quantifies how material deformation varies with different punch speeds, reflecting the capacity of materials to deform plastically at varying tableting speeds. Originally proposed by Roberts and Rowe, the SRS is calculated based on the mean yield pressure (P_y) of pharmaceutical powders when compressed at different punch speeds (*e.g.*, 0.033 and 300 mm/s). Roberts and Rowe found that in CS and polymer materials, an increase in the yield pressure was observed with increasing punch speed, with SRS values of 49.3 and 54.1%, respectively. In contrast, no change in the yield pressure was observed for materials such as heavy magnesium carbonate and calcium carbonate as the punch speed increased. SRS has been widely employed to assess the punch speed-dependent deformation of pharmaceutical powders, with many studies reporting its use in both active pharmaceutical ingredients and excipients.[20–27] SRS is useful for comparing the punch speed-dependent deformation sequences of raw materials; however, the underlying mechanism is not fully understood. SRS is based on the compressive behavior of the powder during the loading process, as both viscoelasticity and plasticity contribute to this behavior.

Stress relaxation refers to the gradual reduction in stress in a material subjected to constant strain, offering insights into its viscoelastic properties. The behavior of pharmaceutical materials during uniaxial compression, such as tableting, involves a combination of plastic deformation and plastic flow. Plastic flow phenomena have been assessed through stress relaxation tests, which measure the evolution of stress when a material is held under constant strain.[28] This helps to determine the rheological properties of the material, including viscoelasticity.

Although the importance of the time- and speed-dependent deformation properties of pharmaceutical materials, such as plastic flow and stress relaxation, is widely recognized, their use as indicators has not yet been clarified. It is challenging to separate the contributions of viscoelasticity and viscoplasticity in the compression process of pharmaceutical raw materials; however, Desbois *et al.* succeeded in separating and evaluating the viscoplasticity of pharmaceutical powders using the jump test, which is widely employed in metallurgy.[7]

Viscous behavior is most pronounced during the compression and decompression stages, influencing material flow and plastic deformation. This study focused on the phenomena that occur in the die from loading to unloading by comparing SRS, mechanical energy, and stress relaxation using four materials known to exhibit different deformation behaviors. The purpose of this study was to understand the characteristics of each method and clarify its usefulness as an indicator for evaluating time-dependent deformation behavior specific to raw materials.

Results and Discussion

SRS Table 1 presents P_y and SRS for the four materials compressed by linear displacement of the punch at speeds of 0.5 and 100 mm/s. The P_y value obtained using the in-die method served as an indicator of plasticity, with lower P_y

Table 1. Strain Rate Sensitivity Based on In-Die Heckel Analysis

Materials	Compression pressure (MPa)	P_y (MPa)		p-Value	SRS (%)
		0.5 mm/s	100 mm/s		
LAC	50	78.4 ± 2.0	81.3 ± 2.0	n.s.	3.6
	100	125.7 ± 4.7	129.6 ± 5.4	n.s.	3.0
	200	152.7 ± 8.4	156.7 ± 7.7	n.s.	2.6
DCPD	50	135.5 ± 1.3	133.7 ± 6.0	n.s.	1.4
	100	243.1 ± 4.2	245.7 ± 7.6	n.s.	1.1
	200	445.6 ± 10.2	451.5 ± 22.8	n.s.	1.3
CS	50	54.2 ± 3.1	78.2 ± 3.5	<0.001	30.7
	100	50.8 ± 2.5	74.8 ± 1.6	<0.001	32.1
	200	51.1 ± 4.9	70.9 ± 1.3	<0.01	27.9
MCC	50	60.2 ± 0.7	71.0 ± 0.7	<0.001	15.2
	100	69.4 ± 1.6	76.7 ± 0.9	<0.01	9.5
	200	99.7 ± 6.8	98.2 ± 5.4	n.s.	1.6

Mean ± standard deviation (S.D.), $n=3$. Statistical analysis was performed using Student's t-test. n.s.: not significant.

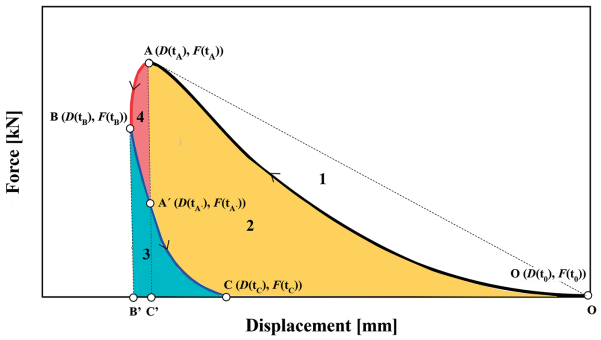

Fig. 1. *AUC* of a Typical Compression Force–Displacement Curve and Associated Mechanical Energy

1: Rearrangement energy; 2+4: plastic energy; 3: elastic energy; and 4: plastic flow energy.

values indicating easier material deformation. DCPD, a typical brittle material, exhibited the highest P_y among the four materials. LAC, CS, and MCC are considered elastic/plastic materials, although their degrees of elasticity and plasticity differ. CS demonstrated the lowest P_y owing to its dominant elastic properties.

The P_y of LAC, DCPD, and MCC increased with compression pressure. However, for CS, there was minimal difference in compression pressure at a punch speed of 0.5 mm/s. In a powder bed, the force applied by the punch is transmitted to individual particles. At low pressures, the particles initially move and rearrange. Once the interparticle gaps become sufficiently small, deformation occurs according to the characteristics of each particle, including particle fracture, plastic, and elastic deformation. This mechanism causes nonlinearity in the OA path of the force–displacement curve in Fig. 1, a phenomenon observed when granular materials, rather than uniform solid materials, undergo uniaxial compression in a die. For CS, the minimal difference due to the test pressure is likely attributed to elastic recovery occurring alongside particle deformation during compression at low punch speeds.

SRS was compared using the P_y values at different punch speeds. DCPD, a brittle material, showed negligible sensitivity to punch speed, with the SRS of approximately 1%. Although the SRS of LAC was higher than DCPD, no significant difference was observed between the P_y values used in the calculation, indicating that its deformation behavior was not affected by punch speed. CS exhibited the highest SRS, ranging from 27.9 to 30.7%, followed by MCC. While SRS depends on the difference between the punch speed levels, the SRS values obtained for the four materials using the trapezoidal punch-displacement profile in this study were consistent with findings from other studies.[19,29] SRS indicates the rate dependence of raw materials; however, separating the viscoelasticity and viscoplasticity of substances is challenging. CS demonstrates a higher SRS than MCC, which necessitates the consideration of both viscoplastic and viscoelastic contributions. While individual CS particles exhibit elastic properties, MCC is fibrous and plastic, undergoing particle entanglement and deformation in response to applied pressure. It is known that the P_y of lactose and MCC is affected by the physical properties (particle size, density, *etc.*) of the excipients,[30–32] even if they have the same components, and the degree of gelatinization or source also affects the P_y of starch.[20] These findings suggest that the physical properties of raw materials affect the intrinsic properties, such as stress relaxation, which will be discussed later. Conversely, it has been reported that the four components, LAC, DCPD, CS, and MCC, can be distinguished by SRS regardless of particle size.[33] Therefore, it is expected that the components of powdered raw materials can be evaluated by expressing the characteristic values affected by compression speed or time dependence as an index.

Mechanical Energy-Associated Compression Figure 2 shows the effect of the punch speed on the plastic and elastic energies of the four materials. Since the plastic flow energy corresponds to the amount of work generated during the stress relaxation phase in the tableting cycle, it was represented as a ratio to plastic energy, as shown in Fig. 3. The elastic energy of DCPD remained unaffected by the punch speed; however, the elastic energies of LAC, CS, and MCC decreased slightly at high speeds. Some tableting issues that occur during the scale-up of the tableting process are thought to be due to the decreased compression time resulting from the increased compression speed. To bridge the gap between this understanding and the observed phenomenon of increased plastic energy and decreased elastic energy at high punch speeds in this study, it is necessary to focus on the punch-displacement waveform used

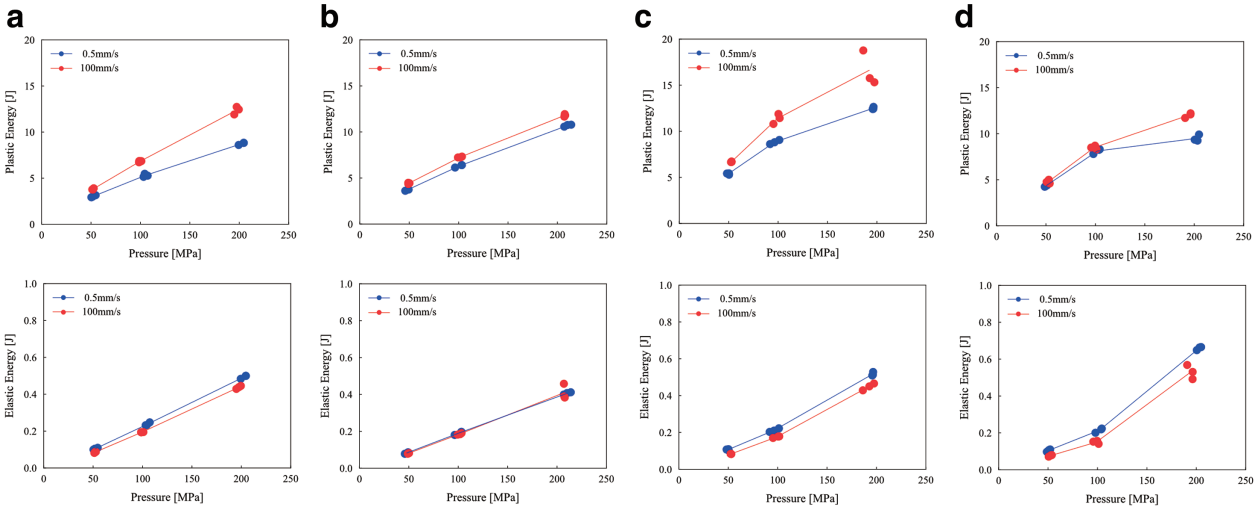

Fig. 2. The Effect of Punch Speed on the Plastic and Elastic Energies of 4 Materials: (a) LAC, (b) DCPD, (c) CS, and (d) MCC

The blue and red colors represent punch speeds of 0.5 and 100 mm/s, respectively, while the lines indicate the average value for each data point.

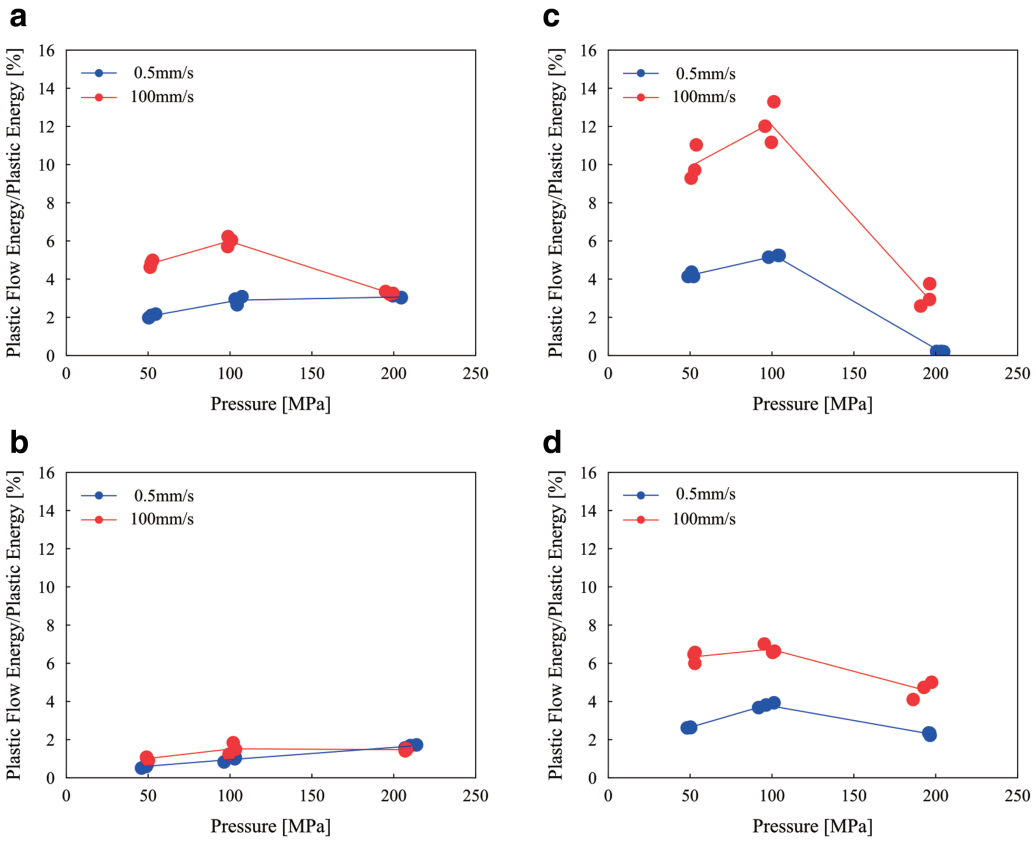

Fig. 3. The Effect of Punch Speed on the Ratio of Plastic Flow Energy to Plastic Energy for 4 Materials: (a) LAC, (b) DCPD, (c) CS, and (d) MCC

The blue and red colors represent punch speeds of 0.5 and 100 mm/s, respectively, while the lines indicate the average value for each data point.

in the material compression test. Much previous research aimed at assessing the deformation properties of pharmaceutical materials has used the saw-tooth waveform as the time-displacement profile of punches. The saw-tooth waveform is characterized by the fact that the speed of the loading and unloading punches is constant and that the dwell time is zero. For this reason, the saw-tooth waveform is applied when evaluating the effect of punch speed on the compression characteristics of powders. However, when the aim is to assess the plastic flow and stress relaxation that occur during the dwell time, the saw-tooth waveform, which has a zero dwell time, is not considered appropriate. Therefore, in this study, a trapezoidal waveform, as shown in Fig. 4, was adopted. As shown in Fig. 4, the typical trapezoidal waveform consists of three steps: loading, dwelling, and unloading. In this study, the loading step was compared at two different punch speeds of 0.5 and 100 mm/s.

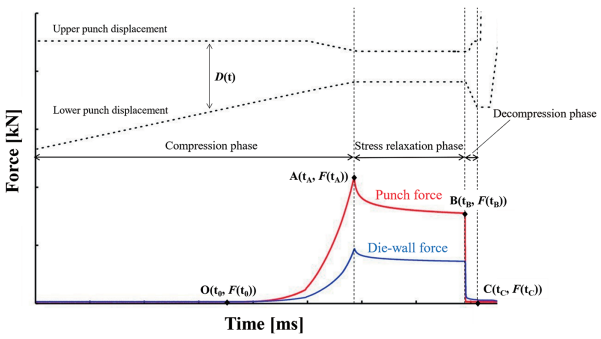

Fig. 4. Representative Force–Time Curve Observed during the Tableting Process Using the Trapezoidal Punch-Displacement Waveform

In both cases, the upper and lower punches were stopped at the position where the maximum stress occurred. Similarly, the upper and lower punches were kept at the position where the maximum stress was reached. In the unloading step, the punch speed was kept constant at 5 mm/s. Therefore, in the trapezoidal waveform applied in this study, only the punch speed in the loading step was changed. As shown in Fig. 3, there were significant differences in the profile of plastic flow energy depending on the material. In the case of DCPD, the plastic flow energy was hardly affected by the punch speed. For the other materials, the plastic flow energy was higher at higher punch speeds, and the order was CS > MCC > LAC. Haware *et al*. applied a trapezoidal waveform to the same materials as in this study under conditions in which the compression pressure was precisely controlled at 103.8 ± 0.8 MPa and evaluated the effects of punch speed and dwell time.[34] A comparison of the in-die Heckel plots obtained at various punch speeds and dwell times revealed a pronounced "nose" in the dwell time for MCC and CS at low punch speeds and long dwell times, but not for DCPD. This nose, attributed to viscosity, disappears at high punch speeds, which is consistent with the findings of the present study. The work required to compress and deform the powder in-die using the upper and lower punches corresponds to plastic energy. Therefore, compared to the saw-tooth waveform, which has a zero dwell time, the trapezoidal waveform, which has a dwell time, adds deformation corresponding to the plastic flow energy, and as in this study, the plastic energy profile may result in the opposite of the saw-tooth waveform.[35,36] Therefore, it is thought that rearrangement accompanied by particle fragmentation and movement occurs during loading in viscous materials such as LAC, MCC, and CS, as shown in Fig. 3. In this study, we did not observe an increase in elastic energy at high punch speeds, which is typically observed with saw-tooth waveforms. As mentioned above, in the trapezoidal waveform used in this study, the impact of the punch speed during loading was evaluated, and the unloading punch speed was set to a constant value regardless of the loading punch speed. Therefore, the impact of the punch speed on the elastic energy profile observed in the saw-tooth waveform was considered to be minimal.

In previous research, the saw-tooth waveform was selected, basically, for the evaluation of time- or speed-dependent compression deformation.[23,37] However, when a sinusoidal waveform was used, such as in a rotary tablet press, the opposite result was obtained.[13,38] Therefore, the unloading punch-displacement profile should be considered when measuring the elastic energy. This consideration is important because the punch profile directly influences the energy distribution during compression and relaxation,[39] affecting the deformation behavior and ultimately the quality of the tablet. This insight underscores the necessity of carefully selecting and controlling the punch-displacement waveform during both the loading and unloading phases, ensuring not only effective research but also the development of robust tablet manufacturing processes.

As shown in Fig. 2, the plastic energy increases or decreases depending on the work performed during the loading and stress relaxation phases, respectively. When comparing the effects of punch speed on plastic energy, it was found that punch speed was not the sole factor affecting plastic energy, and the degree of influence of compression pressure varied depending on the material. For DCPD, which does not exhibit viscoelasticity,[29,40] the effect of punch speed on plastic energy was minimal at all compression pressures. The work that occurs during the stress relaxation phase can be specifically identified as plastic flow energy. The ratios of the plastic flow energies to the plastic energies were compared to characterize the time-dependent deformation behaviors of the 4 materials. Figure 3 shows the effect of the punch speed on this ratio. The plastic flow energy/plastic energy ratio of DCPD remained unaffected by the punch speed. Typically, materials that predominantly undergo brittle fracture during compression are less affected by tableting speed because the brittle fracture is primarily pressure-dependent rather than time-dependent.[9,19,41] Conversely, the plastic flow energy/plastic energy ratios of LAC, CS, and MCC were all higher at a punch speed of 100 mm/s compared to 0.5 mm/s. However, at a compression pressure of 200 MPa, the effect of the difference in the punch speed was less pronounced. This phenomenon can be explained by the increase in the powder bed density with increasing compression pressure. As the powder bed density increases and the particle fracture and flow into gaps reach their limits, the properties of the individual particles become less distinct, and the effects of elasticity become more apparent. Among the four materials used in this study, the porosities of LAC, CS, and MCC approached zero at 100 MPa, whereas that of DCPD approached zero at 200 MPa (data not shown). Leitritz *et al*. studied the elastoplastic behavior of starch through a detailed analysis of force-time curves obtained using an instrumented rotary tablet press.[18] They examined the area of the stress relaxation phase in Fig. 4 of this study and made two important observations. First, tablets do not exhibit excessive elastic recovery as long as significant stress relaxation is detected during the dwell time. Second, at high tableting pressures approaching the porosity limit of the material, there was virtually no plastic flow during the dwell time and elastic compression. The results of our study support these findings even though different raw materials were used. The plastic flow energy of LAC exhibited low sensitivity to variations in pressure and speed. In contrast, the plastic flow energy of CS increased significantly at elevated tableting speeds. Notable differences in tableting speed were evident

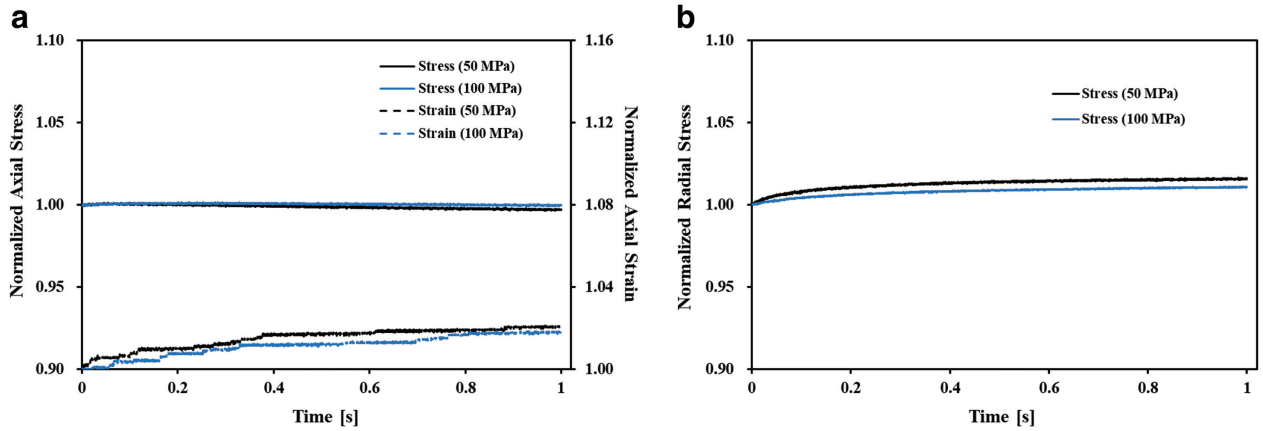

Fig. 5. Changes in Axial Strain and the Relaxation Behavior in (a) the Axial Direction and (b) the Radial Direction during the Stress Relaxation Test at Various Peak Compression Pressures for Rubber

The dotted lines represent strain, while the solid lines indicate stress.

at compression pressures between 50 and 100 MPa. Although MCC also demonstrated an increase in the plastic flow energy at higher punch speeds, the effect was less pronounced than that of CS. Typically, materials that predominantly undergo brittle fracture during compression are less affected by tableting speed because the brittle fracture is primarily pressure-dependent and not time-dependent. This study, which utilized 3 excipients with varying deformation characteristics, suggests that plastic flow energy can effectively elucidate the influence of tableting speed on the compression properties of raw materials.

Axial and Radial Stress Relaxation Behavior Rubber, a typical viscoelastic material, exhibits increasing strain over time during stress relaxation. Even when the stress is held constant, the strain in rubber increases owing to the rearrangement of the molecular chains. As shown in Fig. 5, rubber demonstrated negligible axial stress relaxation. However, the radial stress increased slightly in proportion to the strain increase, with the degree of strain increase being lower at lower compression pressures. This phenomenon may be attributed to the nonlinear elasticity and volume invariance of rubber. Because the rubber volume remains relatively constant during compression, axial stress is maintained. Radial stress increases as the rubber expands radially due to axial forces. Furthermore, in nonlinear materials such as rubber, internal molecular chains harden as strain progresses (strain hardening), potentially suppressing the strain increase at high stress levels. Although the deformation behavior of rubber under compression is complex, it serves as a model for viscoelastic stress relaxation testing in this study.

Figures 6–9 and Table 2 show the stress relaxation curves and strain changes in the axial and radial directions for the four materials examined. We first discuss the effects of the punch speed and compression pressure on the stress relaxation for each material. Among the four materials, DCPD exhibited the least stress relaxation in both the axial and radial directions. Unlike rubber, DCPD exhibits a stress relaxation of approximately 1–5% per second in both directions. The stress relaxation behavior for DCPD was nearly indistinguishable between punch speeds of 0.5 and 100 mm/s. Desbois *et al.* conducted uniaxial compression tests on non-viscoelastic materials containing LAC and DCPD at various speeds, revealing viscoplasticity during the compression process.[4,7] They also demonstrated that the effect of plastic deformation depended on the compression pressure, with the degree of this effect being LAC > DCPD. In the present study, the axial stress relaxation of DCPD and LAC, as shown in Figs. 6 and 7, aligns with the findings of Desbois *et al.* At a punch speed of 0.5 mm/s, stress relaxation in both the axial and radial directions decreased with increasing compression pressure. Additionally, at a punch speed of 100 mm/s, the stress relaxation decreased in both directions.

For LAC, the stress relaxation in both the axial and radial directions was greater than that of DCPD and decreased with increasing compression pressure. This trend was similar in the radial direction. At a punch speed of 100 mm/s, the axial stress relaxation increased at all compression pressures. In contrast, there was no radial stress relaxation in LAC at a compression pressure of 200 MPa. The ratio of plastic flow energy to plastic energy in Fig. 3 indicates that the difference in punch speed disappeared at a compression pressure of 200 MPa, which was also true for stress relaxation. The porosity of the LAC in the die was less than 2% at 100 MPa; at 200 MPa, it was overcompressed. Consequently, viscoelasticity is believed to dominate over viscoplasticity in the time-dependent deformation behavior of LAC. This shift in viscosity may cause differences in stress relaxation between the radial and axial directions. Another factor to consider is the effect of the punch-displacement waveform. In this study, a trapezoidal waveform was applied to the punch-displacement waveform. Therefore, when the punch speed is slow, stress relaxation continues even during loading, resulting in smaller stress relaxation after reaching peak pressure at 0.5 mm/s compared to 100 mm/s. For example, it is noteworthy that the time required for LAC displacement to reach 200 MPa differs significantly between 0.5 mm/s (approximately 35 s) and 100 mm/s (approximately 0.16 s).

The axial stress relaxation behavior of both CS and MCC decreased with increasing compression pressure, with the

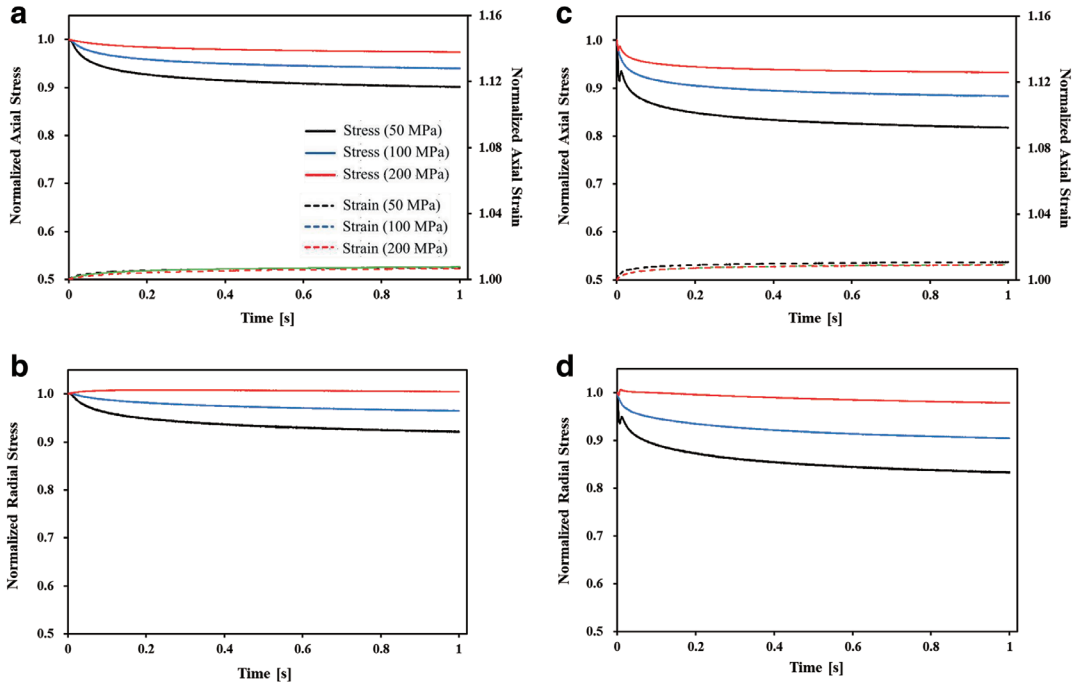

Fig. 6. Changes in Axial Strain and the Relaxation Behavior in the Axial and Radial Directions during the Stress Relaxation Test at Various Peak Compression Pressures for LAC

Panels (a) and (b) represent stress relaxation at a punch speed of 0.5 mm/s, while panels (c) and (d) represent stress relaxation at 100 mm/s. The dotted lines indicate strain, whereas the solid lines represent stress.

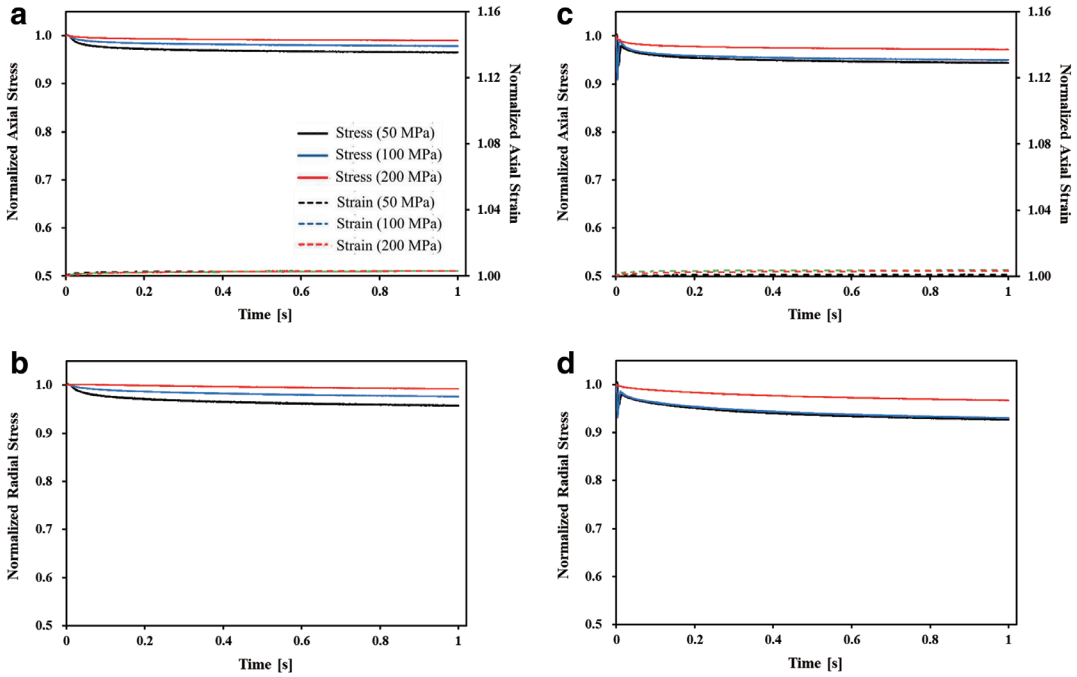

Fig. 7. Changes in Axial Strain and the Relaxation Behavior in the Axial and Radial Directions during the Stress Relaxation Test at Various Peak Compression Pressures for DPCD

Panels (a) and (b) represent stress relaxation at a punch speed of 0.5 mm/s, while panels (c) and (d) represent stress relaxation at 100 mm/s. The dotted lines indicate strain, whereas the solid lines represent stress.

effect being more pronounced in CS. Regarding punch speed, stress relaxation increased at 100 mm/s for both CS and MCC compared to 0.5 mm/s. Notably, an increase in die-wall pressure was observed in CS and MCC at a compression pressure of 200 MPa. At a punch speed of 100 mm/s with CS, an increase in die-wall pressure was observed in CS and MCC at 200 MPa. The increase in die-wall pressure observed in the CS and MCC under high-compression conditions was similar to that of rubber, a viscoelastic material. It is thought that these findings are due to the fact that the

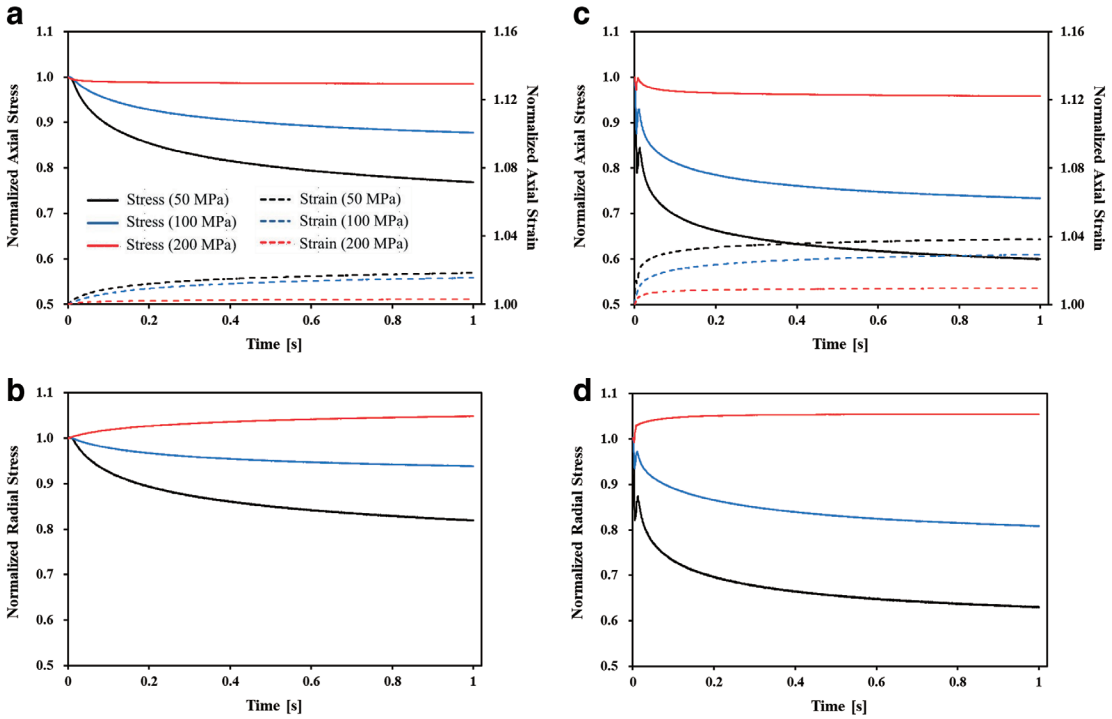

Fig. 8. Changes in Axial Strain and the Relaxation Behavior in the Axial and Radial Directions during the Stress Relaxation Test at Various Peak Compression Pressures for CS

Panels (a) and (b) represent stress relaxation at a punch speed of 0.5 mm/s, while panels (c) and (d) represent stress relaxation at 100 mm/s. The dotted lines indicate strain, whereas the solid lines represent stress.

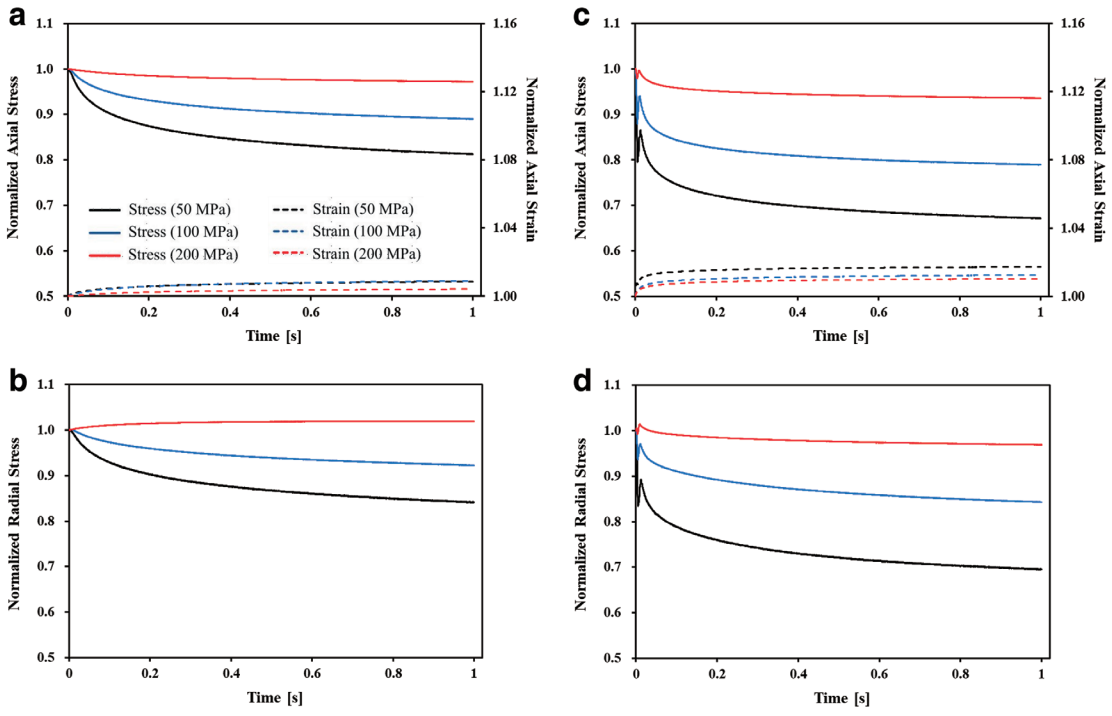

Fig. 9. Changes in Axial Strain and the Relaxation Behavior in the Axial and Radial Directions during the Stress Relaxation Test at Various Peak Compression Pressures for MCC

Panels (a) and (b) represent stress relaxation at a punch speed of 0.5 mm/s, while panels (c) and (d) represent stress relaxation at 100 mm/s. The dotted lines indicate strain, whereas the solid lines represent stress.

elastic properties of both materials became dominant under high compression pressure, causing them to lose their properties as particles. Mazel *et al.* conducted a detailed analysis of the axial and radial stress relaxation behaviors of 4 raw materials (lactose, MCC, pregelatinized starch, and mannitol).[42] From theoretical and experimental perspectives, they elucidated that both viscoplasticity and viscoelasticity occur during stress relaxation.

Table 2. Axial and Radial Stress Relaxation

Material	Punch speed	Compression pressure (MPa)	Normalized stress	
			Axial	Radial
Rubber	0.5 mm/s	50	0.997 ± 0.001	1.016 ± 0.002
		100	0.999 ± 0.001	1.011 ± 0.001
LAC	0.5 mm/s	50	0.900 ± 0.001	0.921 ± 0.002
		100	0.941 ± 0.001	0.965 ± 0.002
		200	0.974 ± 0.000	1.005 ± 0.001
	100 mm/s	50	0.817 ± 0.047	0.833 ± 0.043
		100	0.884 ± 0.000	0.905 ± 0.001
		200	0.933 ± 0.003	0.979 ± 0.016
DCPD	0.5 mm/s	50	0.966 ± 0.001	0.957 ± 0.000
		100	0.980 ± 0.001	0.977 ± 0.000
		200	0.990 ± 0.000	0.992 ± 0.000
	100 mm/s	50	0.944 ± 0.013	0.927 ± 0.017
		100	0.950 ± 0.000	0.930 ± 0.001
		200	0.972 ± 0.012	0.967 ± 0.018
CS	0.5 mm/s	50	0.769 ± 0.004	0.820 ± 0.006
		100	0.874 ± 0.004	0.939 ± 0.005
		200	0.985 ± 0.024	1.048 ± 0.002
	100 mm/s	50	0.600 ± 0.006	0.630 ± 0.008
		100	0.746 ± 0.036	0.809 ± 0.017
		200	0.959 ± 0.005	1.054 ± 0.025
MCC	0.5 mm/s	50	0.812 ± 0.003	0.842 ± 0.004
		100	0.885 ± 0.005	0.923 ± 0.008
		200	0.972 ± 0.003	1.020 ± 0.004
	100 mm/s	50	0.672 ± 0.001	0.695 ± 0.001
		100	0.802 ± 0.034	0.843 ± 0.019
		200	0.935 ± 0.000	0.969 ± 0.065

Mean ± S.D., $n=3$.

The differences in stress relaxation between the axial and radial directions can be attributed to the molecular and structural properties of the materials. In viscoelastic materials, such as rubber, molecular chains reorient under load, leading to anisotropic deformation. Axial compression tends to align the molecular chains along the direction of the applied force, initially minimizing radial movement. However, as the axial force is applied, the internal resistance builds up, resulting in a slight radial expansion as the material strives to maintain volume invariance. In materials such as CS and MCC, the differences in behavior between the axial and radial directions can be attributed to the distribution and rearrangement of the crystalline and amorphous regions. CS with a higher amylopectin content exhibited greater viscoelasticity, resulting in more pronounced stress relaxation and increased die-wall pressure at low punch speeds. In contrast, the behavior of MCC is influenced by hydrogen-bonding networks, which resist compression but exhibit gradual relaxation over time owing to molecular rearrangement. Although DCPD and LAC are sometimes classified as brittle materials, the results of this study demonstrate distinct differences in their deformation characteristics. DCPD, which is characterized by a relatively rigid crystalline structure, shows limited relaxation owing to a reduced number of rearrangeable molecular domains. Conversely, LAC has a lower crystal hardness than DCPD, and because the LAC used in this study was in granular form, it is believed that its relaxation under stress was greater. The porosity observed at 200 MPa indicates that the material reaches a state of over-compression, where further deformation is restricted, leading to reduced stress relaxation in the radial direction. The effects of punch speed and punch-displacement waveform also influence these behaviors. The trapezoidal waveform permits the deformation to continue during the dwell period, thereby promoting time-dependent relaxation. At high punch speeds (*e.g.*, 100 mm/s), the molecular chains have less time to rearrange, resulting in a shift from viscoplastic to viscoelastic behavior. This shift is evident in LAC and CS, where higher punch speeds lead to greater stress relaxation than lower speeds. In contrast, the minimal effect of punch speed on DCPD suggests that the deformation of the material is dominated by plastic flow rather than viscoelastic mechanisms. These molecular and structural insights underscore the importance of understanding anisotropic stress relaxation, as they directly impact tablet quality.

Strain Change During Stress Relaxation Test The stress relaxation test conditions for the compaction simulator were programmed to stop the movement of the upper and lower punches when they reached the maximum compression position. In this study, the change in the distance between the upper and lower punches was measured, and the strain was calculated based on the distance between the punches at the maximum compression position. Stress relaxation testing measures the change in stress over time while maintaining a constant strain. In pharmaceutical research, this test serves as an indicator of the deformation characteristics of raw materials in solid dosage forms. Ideally, the strain of a substance should remain constant during stress relaxation measurements; however, this study observed an increase in strain over time for all four raw materials tested. Figure 10 shows

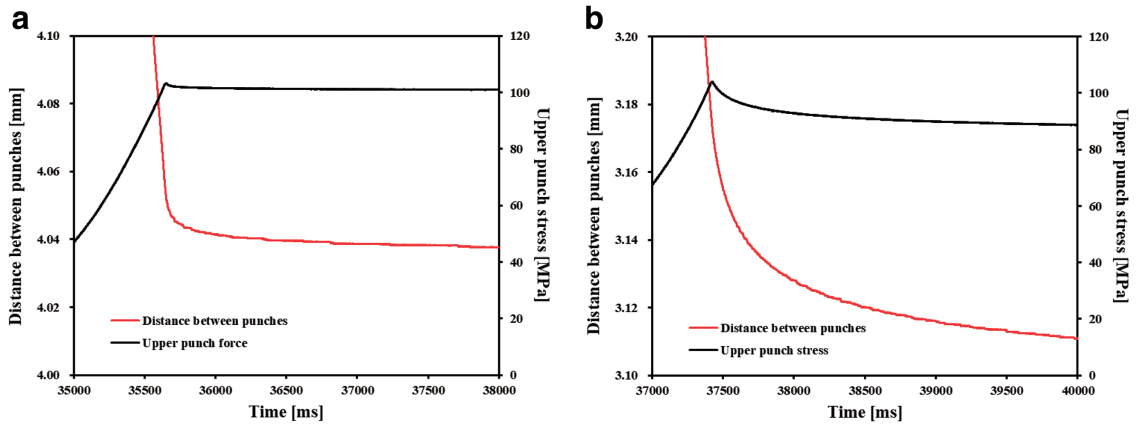

Fig. 10. Typical Stress Decay and Distance between Upper and Lower Punches during the Dwell Phase
(a) DPCD and (b) CS at a punch speed of 0.5 mm/s.

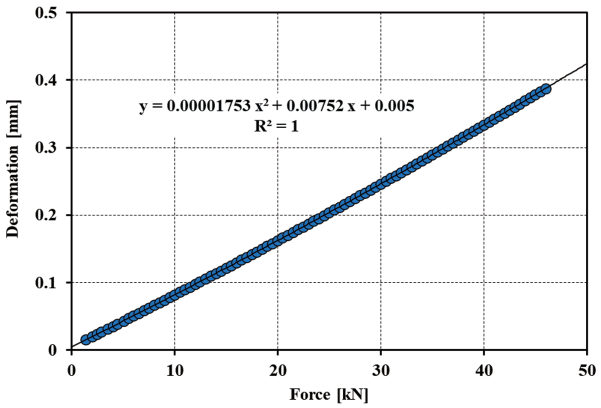

Fig. 11. Calibration Curve of Machine Deformation

the time course of the stress and of the distance between the punches during the stress relaxation test in the DPCD and in the CS as typical examples. The change in strain during stress relaxation varies depending on the material. At a compression pressure of 200 MPa, the granular materials in the die are fully compacted, leaving no gaps and resulting in over-compression. Therefore, this discussion focuses on the results obtained at compression pressures of 50 and 100 MPa.

1) Materials with Minimal Strain Changes: For DCPD and LAC, the strain increase during the first second of the stress relaxation test was less than 1%, with negligible differences observed between punch speeds of 0.5 and 100 mm/s.
2) Materials with Pronounced Strain Changes: In contrast, CS exhibited strain increases ranging from 2.7 to 4.0%, whereas MCC demonstrated increases of 1.0 to 1.7%. The effect of punch speed was particularly significant for both CS and MCC, indicating that these materials are more sensitive to changes in punch speed, likely due to their higher viscosity.

Altaf and Hoag reported that mechanical deformation affects powder deformation behavior in the die during compression and unloading processes in their study using an instrumented rotary press.[43] Several researchers have emphasized the importance of correcting for mechanical deformation when evaluating powder materials' deformation characteristics using compression tests.[44–47] In this study, we introduced a correction formula for mechanical deformation across the test pressure range and conducted our analysis accordingly. As shown in Fig. 11, the error due to mechanical deformation can reach several hundreds of micrometers. However, if Young's modulus of the metal (*e.g.*, stainless steel) used in the tablet press is approximately 200 GPa, the elastic deformation of the machine in the test pressure range of 50–200 MPa is 2.5 to 10 μm. It is likely that the elastic deformation of the machine was not due to distortion of the punch or the tableting machine frame itself; rather, the punch moved physically in the direction of the load. In a uniaxial compression testing machine, such as a compaction simulator, the punch is attached to a holder and positioned such that the punch head contacts the load cell. In rotary tablet presses, the punch moves along the cam track and is not completely fixed to the cam track. The Young's modulus of pharmaceutical raw materials is an order of magnitude smaller than that of metals[48]; therefore, the effect of the elastic deformation of the machine on the long-term deformation behavior of the powder in the die is likely minimal.[7] However, in the early stages of the stress relaxation test, the instantaneous elastic recovery of the machine may cause the stress relaxation to progress more rapidly. This effect was more pronounced at higher punch speeds. The material of the die was stiffer than the punches, and it was assumed there was no movement in the radial direction. Consequently, the amount of mechanical deformation in the radial direction is smaller than that in the axial direction and can be considered negligible.

As shown in Fig. 5, a strain increase of 1–2% was observed in the natural rubber during the stress relaxation test. Creep is a phenomenon in which the strain increases over time when a material is subjected to a constant load. In this study, the increase in strain during stress relaxation reflects a combination of material creep and machine-induced deformations. The strain resulting from creep can be classified as either elastic or inelastic, with the latter encompassing plastic strain. Rubber, being a viscoelastic material, exhibits elastic strain during stress relaxation tests. Conversely, the strain increase observed in CS and MCC may result from a combination of viscoelastic and viscoplastic effects. Consequently, axial stress relaxation

Table 3. Physical Properties of Samples

Materials	Lactose monohydrate	Dicalcium phosphate dihydrate	Cornstarch	Microcrystalline cellulose
Product name	Dilactose S	DI-CAFOS D160	Amidon de Mais B	Ceolus PH-301
True density (g/mL)	1.552 ± 0.001	2.566 ± 0.004	1.535 ± 0.003	1.625 ± 0.003
Particle size (μm)				
D_{10}	37 ± 1	96 ± 6	9 ± 0	22 ± 1
D_{50}	83 ± 4	162 ± 8	15 ± 0	60 ± 2
D_{90}	183 ± 10	236 ± 9	24 ± 1	113 ± 2
Bulk density (g/mL)	0.51 ± 0.01	0.79 ± 0.01	0.55 ± 0.01	0.42 ± 0.01
Tapped density (g/mL)	0.67 ± 0.01	0.90 ± 0.01	0.72 ± 0.02	0.57 ± 0.00

Mean ± S.D., $n=3$.

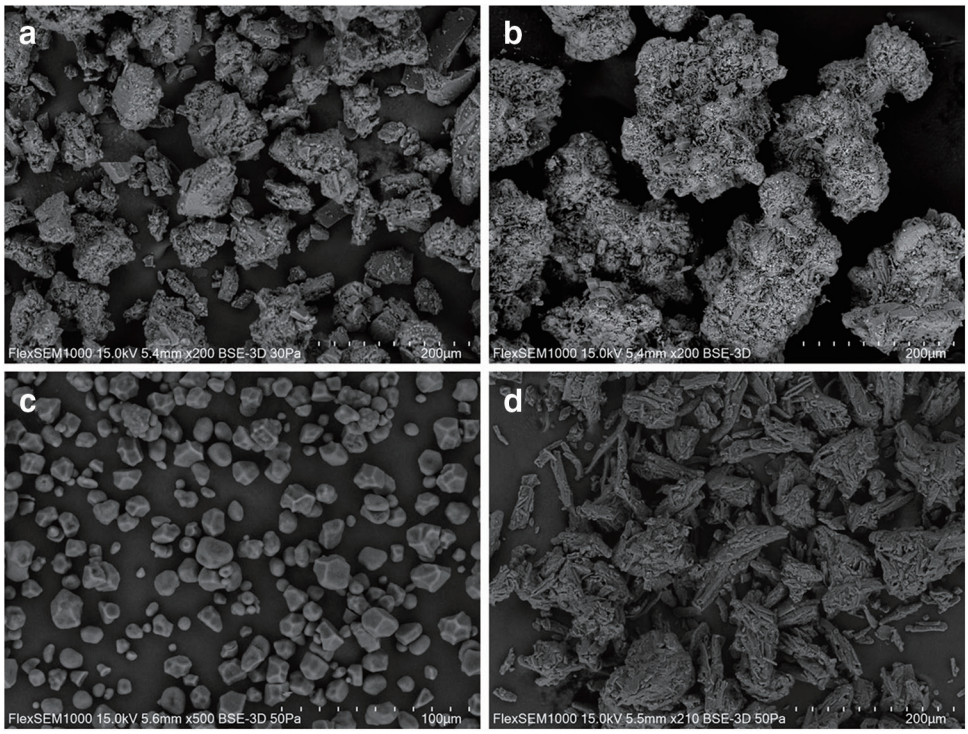

Fig. 12. Scanning Electron Microscope Images of the Samples
(a) LAC, (b) DPCD, (c) CS, and (d) MCC.

has limitations as an indicator for evaluating the deformation behavior of materials, including their viscosity.

Conclusion

In this study, four pharmaceutical excipients—DCPD, LAC, CS, and MCC—with distinct compression deformation properties were evaluated using a compression cycle with a trapezoidal waveform, where only the punch speed during loading was varied. The SRS results were consistent with previous reports, with DCPD and LAC showing no SRS, whereas CS exhibited a high SRS. For DCPD and LAC, it was possible to distinguish between the time-dependent deformation properties of the two materials using an evaluation method based on the ratio of plastic flow energy to plastic energy and stress relaxation as indices. In all evaluation methods for SRS, mechanical energy, and stress relaxation, the compression condition near zero-porosity causes the properties of the compact to become more dominant than the inherent deformation characteristics of the raw material powder or granules. When analyzing the deformation behavior of the raw material, the compression pressure should be selected to preserve the porosity of the material. The time-dependent deformation behavior influenced by mechanical energy and stress relaxation is directly affected by the applied punch-displacement profile. At the punch speed of 0.5 mm/s, deformation progresses over time during loading, which may reduce measurement sensitivity. CS and MCC exhibited an increase in axial strain over time, along with stress relaxation. This effect was nearly negligible for DCPD and slight for LAC compared with CS. Notably, radial stress relaxation was pronounced at high punch speed for CS, which is believed to be due to the viscoelastic effect.

To accurately evaluate the time-dependent deformation characteristics of raw materials, it is essential to select a compression pressure and punch-displacement waveform that considers the porosity of the raw material powder. Even with identical ingredients, the deformation characteristics may vary depending on the particle size and whether granulation has been performed. This study highlighted the significance of punch speed, material properties, and punch-displacement profile on the deformation behavior of pharmaceutical powders. These findings offer valuable guidelines for optimizing R&D and manufacturing high-quality tablets.

Experimental

Materials The materials used in this study were LAC (Dilactose S, Freund, Japan), CS (Amidon de Mais B, Roquette, France), MCC (Ceolus PH-301, Asahi Kasei, Japan), DCPD (Di-Cafos D160, Budenheim, Germany), and magnesium stearate (Mg-St, vegetable-derived, Taihei Chemical Industrial, Japan). Table 3 summarizes the physical properties of LAC, DCPD CS, and MCC, and their particle shapes are shown in Fig. 12, all of which are commonly used in solid oral formulations. The true density was determined using the nitrogen gas displacement method (Pentapycnometer PPY-15 T, Quantachrome, Germany). The particle size was measured using the laser diffraction particle size distribution analyzer (LDSA-1500A, Tohnichi Computer Applications, Japan). The powder tester (MultiTester MT-1001k, Seishin Enterprise, Japan) was used to measure the bulk density and tapped density. The particle shape was observed with a scanning electron microscope (FlexSEM1000, Hitachi High-Tech, Japan). Natural rubber (GS-05, Wakisangyo, Japan) was used as a representative elastic material. The required thickness was achieved by laminating 1 mm natural rubber sheets.

Powder Compaction Using Compaction Simulator All tests were conducted using a compaction simulator (STYL'One Evolution, Medelpharm, Beynost, France). Flat-faced punches with a diameter of 11.28 mm and an instrumented die were employed. To account for machine deformation, the upper and lower punches were brought into direct contact without powder, and a force of up to 46 kN was applied. The resulting displacement and force data were recorded, and a quadratic function was fitted to these data to model the elastic deformation of the machine (Fig. 11). This correction was subsequently applied to all measurements. The die-wall pressure sensor was calibrated by applying known pressures using a rubber with established mechanical properties, ensuring the accurate measurement of radial pressures during compaction. A saw-tooth waveform is characterized by equal speeds of upper and lower punches during both the loading and unloading phases. Additionally, once the set compression stress is reached, the punch displacement is not maintained, and the punches quickly separate from unloading. The saw-tooth profile is used to analyze the compression behavior of raw materials.[19] Although the saw-tooth waveform is essential for accurately assessing punch speed effects, its rapid decay post-peak pressure inadequately facilitates the investigation of plastic flow and stress relaxation occurring near the peak pressure. In this study, a trapezoidal waveform was employed, wherein only the loading punch speed was variable, whereas the dwell time and unloading punch speed remained constant. In this trapezoidal waveform, the punch speed was set at 0.5 and 100 mm/s. In this study, which used a material with a significant difference in viscoelasticity, such as in this test, it is possible to detect variations in the deformation behavior of the material between the slowest speed of 10 mm/s and the highest speeds of 100–500 mm/s.[35] Therefore, the two punch speeds set in this test were appropriate for evaluation. After the maximum pressure, the movement of upper and lower punches was stopped for 4.5 s. Subsequently, the upper die was raised, and the tablets were ejected. The data sampling interval was set at 0.25 ms. Lubricants are employed to enhance the flow of powder into the die and to reduce the friction between the powder and tooling; however, they significantly impact compressibility. Conversely, the friction between the powder and die-wall influences the results of the evaluation in this study. To reduce friction between the powder and the die-wall and punch surface, Mg-St was sprayed for 1000 ms as a lubricant on the punch and die-wall using an external lubrication system (Medelpharm, Beynost) prior to powder filling into the die. To accurately measure the die-wall pressure, the system was configured such that the center of the tablet aligned with the position of the strain gauge, detecting the die-wall pressure, with powder of 450 mg each loaded into the die using a forced feeder equipped with a stirring paddle. However, due to the higher true density of DCPD compared to other raw materials, the tablet mass was established at 720 mg. Each tablet weight was measured using an electronic balance (CPA224S; Sartorius, Göttingen, Germany).

Heckel Analysis and SRS Evaluation The machine speed sensitivity described in the United States Pharmacopeia Chapter 1062, "Tablet Compression Characterization," is instrumental in evaluating tableting speed during the pharmaceutical formulation development process. In this study, SRS was calculated from the P_y obtained at 0.5 and 100 mm/s. According to the original research, the P_y obtained at 0.033 and 300 mm/s should be utilized; however, this is not requisite.[19] When the punch speed was 300 mm/s, it was challenging to stably record data near the maximum pressure. Despite the speed differential for calculating SRS being 0.5 and 100 mm/s, the time-dependent deformation behavior specific to the material can be evaluated.[26] The P_y was derived from the Heckel equation[49]:

$$\ln\left(\frac{1}{\varepsilon}\right) = KP + A \tag{1}$$

where P and ε represent the mean tableting compression pressure and porosity, respectively. The reciprocal of the slope (K) of the linear portion of the Heckel plot corresponds to the P_y,[50] where A is the intercept at $P=0$ when the line in the Heckel plot is extrapolated. Here, ε is calculated by Equation (2):

$$\varepsilon = 1 - \frac{\text{Tablet weight}}{\left(\text{Tablet volume}/\text{True density}\right)} \tag{2}$$

where the tablet volume was calculated from the diameter and the minimum powder height in the die (distance between the punches).

Definition and Calculation of Mechanical Energy To quantify the work and mechanical energy required for the tableting cycle, the force–displacement and force–time curves are presented in Figs. 1 and 4, respectively. Figure 4 shows a typical force-time curve for a tableting cycle encompassing loading and unloading. This curve can be segmented into three distinct phases.[45,51] The initial phase represents loading, during which the material experiences increasing strain due to the displacement of the upper and lower punches. After this phase, the force reaches its maximum at point A. The subsequent phase involves stress relaxation, characterized by a slight decrease in force from the peak value during the dwell time, defined as the duration required for the flat portion of the punch head to

traverse the compression roller between points A and B. The final phase is unloading between points B and C, marked by a rapid decline in the axial force to 0 as the gap between the punches increases. However, the behavior of the radial pressure may vary based on the raw material, potentially not returning to 0, resulting in a detectable residual die-wall pressure.

Figure 1 shows the force–displacement curve derived from the uniaxial compression test. The displacement, that is, the distance between the punches, corresponds to the tablet thickness in the die. Four types of mechanical energy were identified: particle rearrangement energy, plastic energy, plastic flow energy, and elastic energy. Notably, the plastic flow energy constitutes a subset of the plastic energy. Under ideal conditions, the force–displacement curve should theoretically follow the path OABB′ in Fig. 1 (a linear path between O and A) during material loading and unloading. The path OA is nonlinear due to friction and variations in the contact area between particles.[14] The area designated as the particle rearrangement energy is influenced by the filling depth and was excluded from the evaluation in this study. The area OABB′ represents the compression energy, corresponding to the total work required during the compression phase of the material. Because the punch force in Fig. 4 and the punch displacement in Fig. 1 are expressed as functions of time, $F(t)$ and $D(t)$, respectively, they can be represented by Equation (3). Here, the times t_0, t_A, t_B, and t_C correspond to the respective points shown in Fig. 1. The displacements and forces associated with each time were extracted from the data obtained during the compression test. This process was conducted using compaction simulator control and analysis software (Analis v2.08.8, Medelpharm, Beynost):

$$\text{Compression energy} = \int_{t_0}^{t_B} F(t)\frac{dD(t)}{dt}dt \tag{3}$$

At point B in Fig. 1, the material was unloaded as the distance between the upper and lower punches increased, and the force decreased rapidly (path BC in Fig. 1). The work of the BB′C region corresponds to the volume expansion that occurs when the tablet is unloaded in the die and is calculated using Equation (4):

$$\text{Elastic energy} = \int_{t_B}^{t_C} F(t)\frac{dD(t)}{dt}dt \tag{4}$$

Although the elastic energy yields a negative value, it is presented as an absolute value in this study. Plastic energy is necessary to deform the powder bed irreversibly. Consequently, it is obtained by subtracting the elastic work from the total work and is calculated using Equation (5):

$$\text{Plastic energy} = \text{Compression energy} - \text{Elastic energy}$$

$$= \left|\int_{t_0}^{t_B} F(t)\frac{dD(t)}{dt}dt\right| - \left|\int_{t_B}^{t_C} F(t)\frac{dD(t)}{dt}dt\right| \tag{5}$$

The plastic energy associated with the stress relaxation phase between points A and B in Fig. 4 is defined as plastic flow energy (area ABA′ in Fig. 1) and is expressed by the following Equation (6)[15,52]:

$$\text{Plastic flow energy} = \left|\int_{t_A}^{t_B} F(t)\frac{dD(t)}{dt}dt\right| - \left|\int_{t_B}^{t_A'} F(t)\frac{dD(t)}{dt}dt\right| \tag{6}$$

To compute the 3 mechanical energies, the *AUC* of the force–displacement curve was approximated using the trapezoidal rule. Points A and B in Fig. 1, utilized for calculating the plastic flow energy, correspond to those in Fig. 4. Therefore, the displacement of point A over time in Fig. 1 was first examined, and the point at which the same displacement occurred during the unloading process was designated as A′ in Fig. 1, When calculating the *AUC* of path AB using the trapezoidal approximation, its value is in the area ABB′C′A′, which includes elastic energy. Thus, the area A′BB′C′ was subtracted from area ABB′C′A′ to obtain the plastic flow energy.

Stress Relaxation Test In the stress relaxation test, a constant strain was applied while measuring the stress changes over time. This study involved straining the powder until specific punch pressures (50, 100, and 200 MPa) were achieved at both low (0.5 mm/s) and high (100 mm/s) speeds. However, the strain required to reach each pressure varied depending on the powder. The stress relaxation of the powdered materials did not stabilize even after the test duration. Notably, compression using a rotary tablet press typically occurs within milliseconds to hundreds of milliseconds, which is shorter than the duration of this test. To evaluate the stress relaxation behavior of each material, this study analyzed compression data for the upper and lower punch pressures and die-wall pressure over one second to assess the axial and radial stress relaxation. Stress relaxation can be divided into instantaneous and gradual components that occur after a delay. According to the results of previous research, differences in the deformation behavior of materials during stress relaxation can be observed over a period of one second.[26] The test was conducted in triplicate to ensure reproducibility. The strain within the powder was measured at the upper and lower punch positions during the test. As previously mentioned, the punch force (stress) and strain vary depending on the material. In particular, the data at 100 mm/s fluctuates slightly due to equipment limitations. To mitigate these effects and facilitate the comparison between different materials, the stress and strain were normalized using Equations (7) and (8):

$$\sigma_{Norm} = \frac{\sigma(t)}{\sigma_{Peak}} \tag{7}$$

$$\varepsilon_{Norm} = \frac{\varepsilon(t)}{\varepsilon_{Peak}} \tag{8}$$

where σ and ε represent stress and strain, respectively. The peak stress (σ_{Peak}) value was divided by the stress at time t ($\sigma(t)$) to normalize. The same normalization process was applied to the strain.

Conflict of Interest The authors declare no conflict of interest.

References

1) Aoki S., Uchiyama J., Ito M., *J. Pharm. Sci*., **103**, 235–240 (2014).
2) Train D., *J. Pharm. Pharmacol*., **8**, 745–761 (1956).
3) Casahoursat L., Lemagnen G., Larrouture D., *Drug Dev. Ind. Pharm*., **14**, 2179–2199 (1988).
4) Danjo K., Hiramatsu A., Otsuka A., *J. Soc. Powder Technol*., **35**, 662–670 (1998).
5) Rubinstein M. H., Jackson I. M., *Int. J. Pharm*., **36**, 99–104 (1987).
6) Van der Voort Maarschalk K., Zuurman K., Vromans H., Bolhuis G. K., Lerk C. F., *Int. J. Pharm*., **151**, 27–34 (1997).
7) Desbois L., Tchoreloff P., Mazel V., *Powder Technol*., **404**, 117406 (2022).
8) Nelson E., Busse L. W., Higuchi T., *J. Am. Pharm. Assoc.* (Scientific ed.), **44**, 223–225 (1955).
9) Antikainen O., Yliruusi J., *Int. J. Pharm*., **252**, 253–261 (2003).
10) Gharaibeh S. F., Chick Al-Ard I. N., *Powder Technol*., **214**, 161–168 (2011).
11) Hoblitzell J. R., Rhodes C. T., *Drug Dev. Ind. Pharm*., **16**, 201–229 (1990).
12) Ragnarsson G., Sjögren J., *J. Pharm. Pharmacol*., **37**, 145–150 (1985).
13) Garr J. S. M., Rubinstein M. H., *Int. J. Pharm*., **72**, 117–122 (1991).
14) Tay J. Y. S., Kok B. W. T., Liew C. V., Heng P. W. S., *J. Pharm. Sci*., **108**, 3011–3019 (2019).
15) Yu H. C. M., Rubinstein M. H., Jackson I. M., Elsabbagh H. M., *J. Pharm. Pharmacol*., **40**, 669–673 (1988).
16) Oates R. J., Mitchell A. G., *J. Pharm. Pharmacol*., **41**, 517–523 (1989).
17) Dwivedi S. K., Oates R. J., Mitchell A. G., *J. Pharm. Pharmacol*., **43**, 673–678 (1991).
18) Leitritz M., Krumme M., Schmidt P. C., *J. Pharm. Pharmacol*., **48**, 456–462 (1996).
19) Roberts R. J., Rowe R. C., *J. Pharm. Pharmacol*., **37**, 377–384 (1985).
20) Katz J. M., Buckner I. S., *Int. J. Pharm*., **442**, 13–19 (2013).
21) Doktorovová S., Stone E. H., Henriques J., *AAPS PharmSciTech*, **23**, 96 (2022).
22) Nokhodchi A., Rubinstein M. H., Ford J. L., *Int. J. Pharm*., **126**, 189–197 (1995).
23) Garekani H. A., Ford J. L., Rubinstein M. H., Rajabi-Siahboomi A. R., *Drug Dev. Ind. Pharm*., **27**, 935–942 (2001).
24) Paul S., Tajarobi P., Boissier C., Sun C. C., *Int. J. Pharm*., **566**, 24–31 (2019).
25) Mizunaga D., Koseki M., Watano S., *J. Soc. Powder Technol*., **57**, 577–587 (2020).
26) Mizunaga D., Koseki M., Kamemoto N., Watano S., *Chem. Pharm. Bull*., **69**, 1184–1194 (2021).
27) Roopwani R., Buckner I. S., *J. Pharm. Sci.*, 1–10 (2021).
28) David S. T., Augsburger L. L., *J. Pharm. Sci*., **66**, 155–159 (1977).
29) Rees J. E., Rue P. J., *J. Pharm. Pharmacol*., **30**, 601–607 (1978).
30) Haware R. V., Bauer-Brandl A., Tho I., *Pharm. Dev. Technol*., **15**, 394–404 (2010).
31) Fell J. T., Newton J. M., *J. Pharm. Sci*., **60**, 1866–1869 (1971).
32) Roberts R. J., Rowe R. C., *J. Pharm. Pharmacol*., **38**, 567–571 (1986).
33) Roberts R. J., Rowe R. C., *Chem. Eng. Sci*., **42**, 903–911 (1987).
34) Haware R. V., Tho I., Bauer-Brandl A., *Powder Technol*., **202**, 71–77 (2010).
35) Larhrib H., Wells J. I., *Int. J. Pharm*., **160**, 197–206 (1998).
36) Nokhodchi A., Rubinstein M. H., Larhrib H., Guyot J. C., *Int. J. Pharm*., **120**, 13–20 (1995).
37) Nokhodchi A., Ford J. L., Rowe P. H., Rubinstein M. H., *J. Pharm. Pharmacol*., **48**, 1122–1127 (1996).
38) Akande O. F., Rubinstein M. H., Rowe P. H., Ford J. L., *Int. J. Pharm*., **157**, 127–136 (1997).
39) Muller F. X., Augsburger L. L., *J. Pharm. Pharmacol*., **46**, 468–475 (1994).
40) Meynard J., Amado-Becker F., Tchoreloff P., Mazel V., *Int. J. Pharm*., **613**, 121410 (2022).
41) Çelik M., Okutgen E., *Drug Dev. Ind. Pharm*., **19**, 2309–2334 (1993).
42) Mazel V., Guerard S., Croquelois B., Kopp J. B., Girardot J., Diarra H., Busignies V., Tchoreloff P., *Int. J. Pharm*., **513**, 669–677 (2016).
43) Altaf S. A., Hoag S. W., *J. Pharm. Sci*., **84**, 337–343 (1995).
44) Belda P. M., Mielck J. B., *Eur. J. Pharm. Biopharm*., **47**, 231–245 (1999).
45) Schmidt P. C., Vogel P. J., *Drug Dev. Ind. Pharm*., **20**, 921–934 (1994).
46) Oates R. J., Mitchell A. G., *J. Pharm. Pharmacol*., **42**, 388–396 (1990).
47) Dwivedi S. K., Oates R. J., Mitchell A. G., *J. Pharm. Pharmacol*., **44**, 459–466 (1992).
48) Bassam F., York P., Rowe R. C., Roberts R. J., *Int. J. Pharm*., **64**, 55–60 (1990).
49) Heckel R. W., *Trans. Metall. Soc. AIME*, **221**, 671–675 (1961).
50) Hersey J. A., Rees J. E., *Nat. Phys. Sci.* (Lond.), **230**, 96 (1971).
51) Vogel P. J., Schmidt P. C., *Drug Dev. Ind. Pharm*., **19**, 1917–1930 (1993).
52) Tye C. K., Sun C. C., Amidon G. E., *J. Pharm. Sci*., **94**, 465–472 (2005).